Electrically pumped GeSn micro-ring lasers

Teren Liu, Lukas Seidel, Omar Concepción, Vincent Reboud, Alexei Chelnokov, Giovanni Capellini, Michael Oehme, Detlev Grützmacher and Dan Buca

Abstract—**Recent progress in the quest for CMOS-integrable GeSn light sources comprises the optically-pumped laser operating at room temperature and the first demonstrations of electrically pumped lasers. In this work, the performance of electrically-pumped double heterostructure GeSn ring laser diodes are evaluated as a function of their geometry and pumping pulse time. In particular, the trade-off between the band structure, i.e. the directness of the GeSn band gap, and the device heat dissipation is discussed in terms of their impact on the emission intensity and threshold current density.**

***Keywords* — electrical pumped lasers, GeSn, Si Photonics**

I. INTRODUCTION

For a long time, laser structures on silicon fabricated solely from elements of group IV were considered as the Holy Grail for Si Photonics [1], [2], [3], [4], [5], [6], [7]. With the breakthrough in epitaxial growth of GeSn and SiGeSn group IV semiconductors, the development of laser diodes on Si got a totally new perspective [7], [8], [9], [10], [11]. The Sn incorporation into the Ge lattice reduces the energy level of Γ-valley was faster reduced then the indirect L-valley of conduction band transforming the indirect bandgap Ge into a direct band gap alloy. In contrast, adding Si into the GeSn alloys has the opposite effect increasing the direct bandgap energy, even transforming the alloy back into a indirect semiconductor. This band structure tuning of SiGeSn ternary alloy offers a large flexibility for active optical gain media from simple bulk GeSn layers to complex quantum well GeSn/SiGeSn heterostructures [10], [12], [13], [14]. In addition to the Si and Sn alloying, the electronic band structure can be further manipulated via lattice strain engineering, a technology well developed in the Si nano-electronics field.

The strain and the alloy stoichiometry defines the energy separation between the Γ- and L-valley quantity termed as "directness". A large directness decreases the electron intraband scattering rate from the low density of states (DOS) Γ- valley into the larger DOS L-valleys and increases the radiative recombination efficiency in the active optical layer [13], [14], [15], [16], [17].

Different optical pumped GeSn laser designs have been reported lately including uniaxial strained micro-bridges [18], [19], [20], biaxially compressive and tensile strained micro-disks [8], [9], [10], [11], [21], [22], [23], [24], photonic crystals [25], [26], [27] and Fabry-Pérot (FP) waveguide cavities [10], [28], [29], [30]. Within few years, the lasing operating temperature was increased from 90 K to 300 K and the laser threshold, at cryogenic temperature, decreased from 300 kW/cm^2 to 0.8 kW/cm^2 [8], [9], [10], [11], [15], [20], [22], [23], [25], [30], [31], [32], [33], [34], [35]. The learning from these studies together with knowledge gained from GeSn electronics [36], [37], [38] forms a solid base for addressing the next challenge: the electrical pumped laser. Indeed, achieving an electrically pumped GeSn laser is a much more challenging task, as it requires more elaborated layer stacking for carrier injection as well as suitable solutions for low-resistance electrical contacts and heat dissipation management [39].

Recently, electrical pumped lasers were demonstrated in SiGeSn/GeSn/SiGeSn double heterostructure (DHS) [40], [41], [42], [43]. However, the lasing effect, observed only for below µs electrical pulse length and large injection currents, requires additional studies to understand the influence of the material and cavity losses on key parameters like lasing threshold, output power or maximum operating temperature. This paper compares the laser characteristics of electrically-pumped ring laser diodes featuring different cavity designs and dimensions and discussed the role of the active layer lattice strain and heating on the laser performance.

Manuscript received May 31st, 2024; revised September 13th, 2024; accepted May 3rd, 2024. Date of publication ####; date of current version ####. The authors acknowledge financial support from the European Commission for the LASTSTEP Project under grant agreement 101070208 and the German Research Foundation (DFG) under Projects "Thermoelektrische Eigenschaften von SiGeSn-Mikrobauelementen" (Corresponding authors: Teren Liu and Dan Buca).

Teren Liu, Omar Concepción, Detlev Grützmacher and Dan Buca are with Peter-Grünberg-Institute (PGI-9) and JARA-Fundamentals of Future Information Technologies, Forschungszentrum Jülich, Germany. (emails: t.liu@fz-juelich.de; o.diaz@fz-juelich.de; d.gruetzmacher@fz-juelich.de; d.m.buca@fz-juelich.de)

Lukas Seidel and Michael Oehme are with Institut für Halbleitertechnik, University of Stuttgart, Germany. (emails: lukas.seidel@iht.uni-stuttgart.de; michael.oehme@iht.uni-stuttgart.de)

Vincent Reboud and Alexei Chelnokov are with CEA-Leti, Grenoble, France. (emails: vincent.reboud@cea.fr; alexei.tchelnokov@cea.fr)

Giovanni Capellini is with Dipartimento di Scienze, Università Roma Tre, Roma, Italy and IHP Leibniz Institut für innovative Mikroelektronik . (e-mail: capellini@ihp-microelectonics.com)

Color versions of one or more of the figures in this article are available online at http://ieeexplore.ieee.org

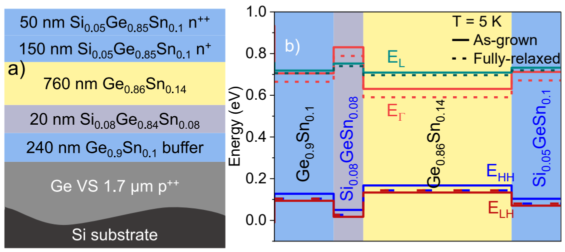

***Figure 1**: (a) Sketch of a epitaxialy grow p-i-n SiGeSn/GeSn/SiGeSn/Ge-VS/Si(100) DHS as used for laser diode fabrication. (b) Electronic band structure simulation of the heterostructure from (a) for the as-grown and fully strain relaxed cases.*

II. Main

The p-i-n SiGeSn/GeSn/SiGeSn/Ge heterostructure was grown in an industry-compatible reduced-pressure chemical vapor deposition reactor on 200 mm Si wafers, as shown in Fig. 1a. A 200 nm $Ge_{0.92}Sn_{0.08}$ buffer layer was deposited on a 10^{18} cm^{-3} boron doped 2 µm thick Ge-Virtual Substrate (Ge-VS). The plastically-relaxed Ge-VS reduces the large crystal lattice difference between the Si and the GeSn layers, enabling the incorporation of higher Sn contents in the GeSn epilayer with a high crystalline quality. The role of an intermediate, strain-relaxed $Ge_{0.9}Sn_{0.10}$ layer is to offer a larger lattice constant, thus reducing the epitaxial compressive strain build-up in the subsequently grown GeSn layers. The optical active $Ge_{0.86}Sn_{0.14}$ layer features a compressive biaxial strain of -0.35% , as determined by X-ray diffraction, and is sandwiched between two SiGeSn layers with a larger bandgap to assure carrier confinement in the optical active region. For efficient electron injection into in the GeSn active layer the top SiGeSn layer consist of a low doped,< 10^{18} cm^{-3} region of 150 nm thickness and a top 50 nm highly doped, 5×10^{19} cm^{-3}, layer (see Fig. 1a). Based on k·p modeling the band diagram of the undoped DHS is shown in Fig. 1b [14], [44], indicating an band offset energy confinement of ~ 60 meV.

For the characterization of the optical-active material, non-undercut circular shaped LEDs were fabricated as described in the Methods section. Electroluminescence (EL) measurements of the LEDs were performed in the temperature range from 5K to 295K and current density

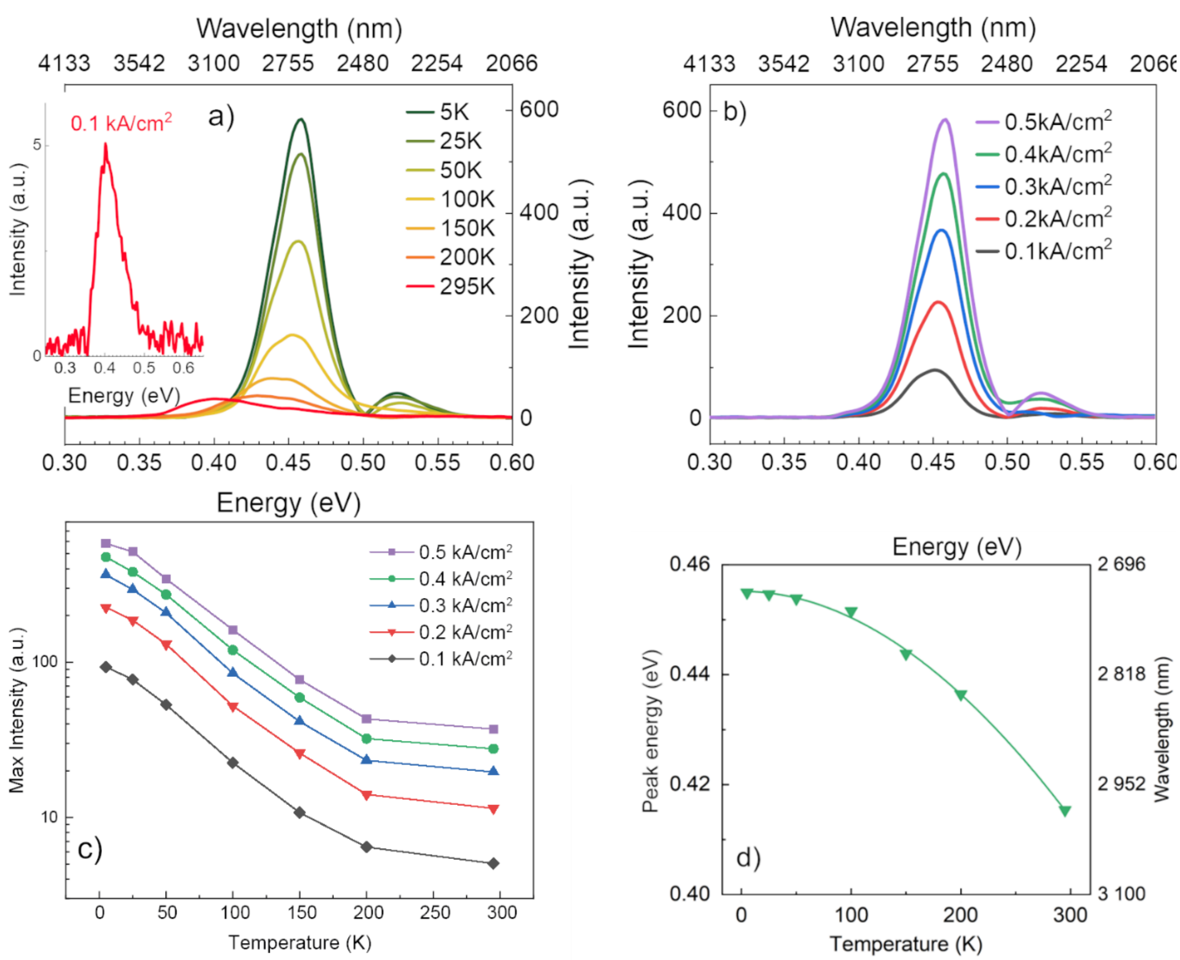

***Figure 2**: (a) LED emission spectrum using a current density of 0.5 kA/cm² at different temperatures. The inset is 0.1 kA/cm² at RT. (b) Emission spectrum at 5K under different current densities. (c) Log scale maximum intensity of the LED emission of the p-i-n DHS at different current densities. (d) Peak energy of the GeSn LED measured at different temperatures.*

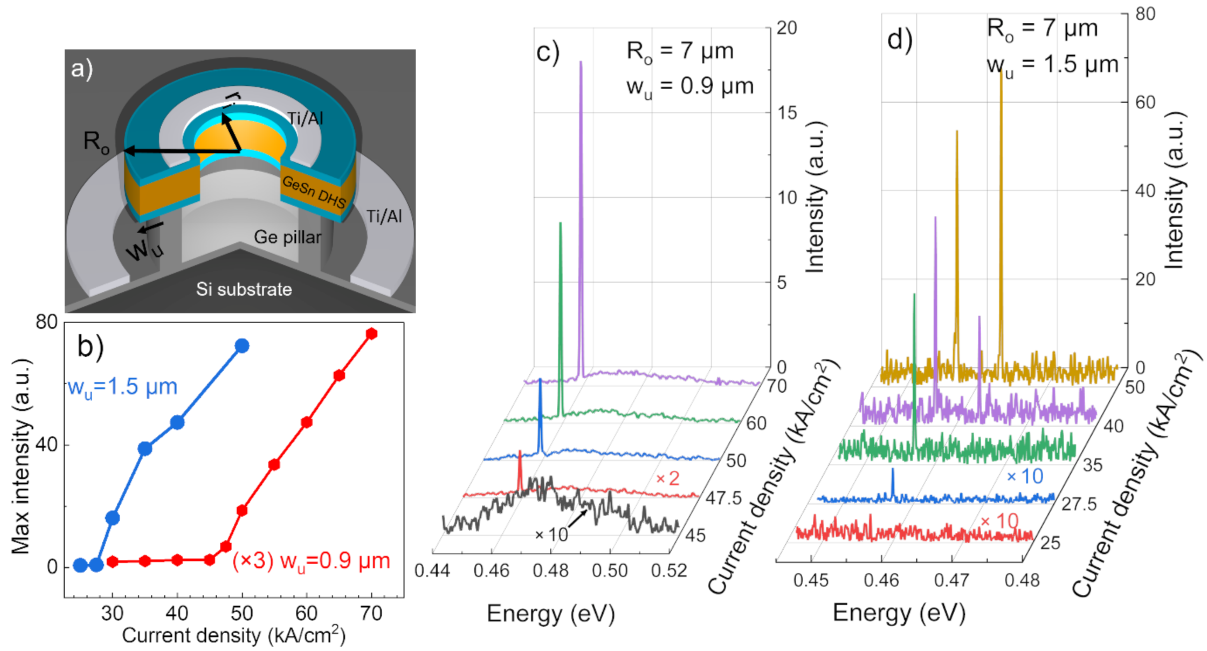

***Figure 3**: (a) Schematic of an undercut GeSn ring laser diode. (b) The L-I characteristics of both laser diodes. (c,d) Current density dependent spectra of 7 µm outer radius micro disk laser diode with (b) 0.9 µm and (c) 1.5 µm undercut width. For 1.5 µm undercut, a second lasing mode appears at 40 kA/cm^2.*

range from 0.1 kA/cm^2 to 0.5 kA/cm^2 at 2 kHz and 50% duty cycle pumping condition (Figs. 2a, b). The diodes emit in mid-infrared with a peak wavelength of 2.7 µm at 5K and different current densities, in agreement with the $k \cdot p$ modeling (Fig. 1b). At room temperature (RT) the EL intensity drops to 5% of the emission at 5K under the same pumping condition (Fig. 2c). The peak energy decreases by 30 meV from 5K to RT, following the Varshni equation behavior, as shown in Fig. 2d [45]. The temperature dependence of the LED emission indicates a typical direct bandgap semiconductor behavior: the emission intensity strongly increases with decreasing temperature [10].

The non-undercutted LEDs (Fig.3a) exhibit measurable RT spontaneous emissions down to a pumping current density of 100 A/cm^2, due to the limit of our electronic set-up. Their emission can be further improved by strain engineering. As discussed in the introduction section, the compressive strain has a negative impact on “directness”, leading to a lower energy separation between the Γ- and L-valley. To promote the strain relaxation of the GeSn layer in the rim region, where the Whispering Gallery Modes (WGMs) develop, the Ge virtual substrate was selectively etched to a variable lateral width, w_u. As recently demonstrated in similar GeSn disk diodes, the under-etching of the Ge-VS buffer, allows nearly-full relaxation of the residual compressive strain in the GeSn layer [46], In addition to the resulting increased directness and reduced bandgap, the presence of an undercut also improves the optical mode confinement in the rim region. According to previous published study of GeSn refractive index [47], the undercut also creates a much larger refractive index contrast n_{GeSn}/n_{air}: 4.39/1, comparing to refractive index contrast in non-undercut GeSn/Ge structure n_{GeSn}/n_{Ge}: 4.39/4, which achieved an excellent value of the mode overlap of 0.98 from simulation. With the improvement of band structure and optical cavities, laser emission was obtained from the vertical GeSn diodes.

A sketch of laser diode cavity is presented in Fig. 3a, describing the main geometric parameters including undercut widths (w_u), inner radii (r_i), and outer radii (R_o). The WGMs are formed at the outer rim of the micro-ring, and the removal of the center part of a disk was reported to increase the laser emission intensity, reduce the threshold current density as well as the background emission when compared to a micro-disk geometry with the same outer radius [42]. For small devices up to $R_o = 10$ µm, the inner hole radius was chosen to be $r_i = 1$ or 2 µm, while for devices with larger R_o, the center hole radius was increased ($r_i = 9$ µm for $R_o = 20$ µm and $r_i = 18$ µm for $R_o = 40$ µm devices, respectively).

The L-I laser characteristics, and 3D plots of the emission spectra versus current density for two laser diodes with different undercut widths of $w_u =$ 0.9 µm and $w_u = 1.5$ µm are presented in Figs. 3b, c, d. Both diodes have an outer radius of $R_o = 7$ µm. The measurements were taken under 100 ns electrical pump pulses at a repetition rate of 50 kHz.

For all laser diodes, a clear transition from spontaneous emission to amplified emission that defines the laser threshold is observed. The laser diode with a smaller GeSn undercut shows a much larger threshold current density of $J_{th} = 48$ kA/cm^2 and the emission spectrum is restricted to only one laser mode at 0.459 eV. The diode with the larger undercut of 1.5 µm shows almost 50% lower threshold, and multimode emission: a main mode at 0.457 eV and a second one at 0.463 eV that appears at a current density > 40 kA/cm^2. For both laser diodes, at the threshold, the

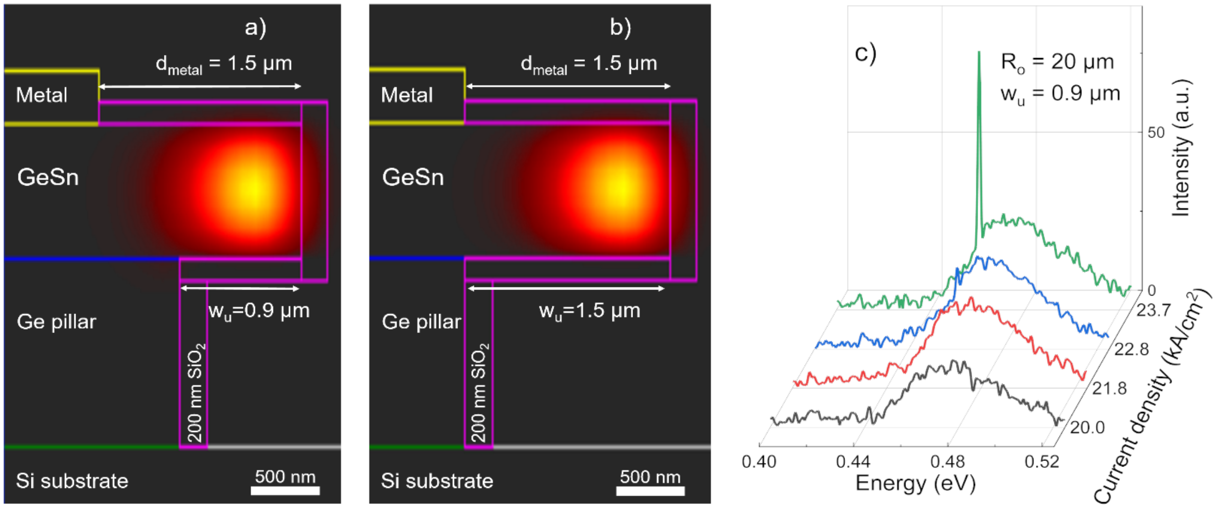

***Figure 4**: (a, b) Simulation of the mode confinement in the GeSn/Ge heterostructure for the 0.9 µm and 1.5 µm undercut micro-ring structures, wavelength of 2.7 µm. (c) Laser spectrum of a diode with 20 µm of outer radius, 9 µm of inner radius, and 0.9 µm of undercut diode.*

linewidth collapses from a FWHM of 40 meV to 0.5 meV, which is close to the limit of the measurement set-up. Note that no apparent device degradation was observed after more than 20 hrs of cumulative measurements.

The large difference in the laser threshold for different undertect length is mainly attributed to two factors: (i) the slightly higher GeSn strain relaxation for the larger undercut, which leads to an increased directness in the GeSn region where the WGMs are formed; (ii) the increase of optical losses for lower undercut diodes due to the optical mode proximity to the Ge pillar (small refractive index difference). A larger directness and a slightly smaller bandgap will not be automatically seen in the laser emission, since the laser mode is also defined by the cavity R_o, which is similar for both diodes.

Supporting information is obtain by simple optical mode modeling in two undercut GeSn/Ge pillar cavities, as shown in Figs. 4a, b. The simulation was performed using the RSOFT FEMSim software at a wavelength of 2.7 µm. Both device designs are identical except for the undercut depth. Due to the lack of experimental data and only a low Si content, the refractive index of the SiGeSn layers was chosen to be the same as the GeSn layer. For the 1.5 µm undercut cavity, the optical mode is fully confined in the GeSn free standing region, while for the 0.9 µm undercut cavity, clear extension of the mode in the Ge pillar region is observed. This may increase the optical losses and decreasing the net gain that leads to higher threshold as well as the vanishing of the second lasing mode for the shorter under-etch case.

For small diode radius below $R_o < 10$ µm, larger undercut cavities shows better laser performances compared to shorter undercut cavities. However, above 10 µm outer radius the diodes show only spontaneous emission and do not reach the lasing threshold, regardless of the pumping conditions, e.g. lower duty cycles or short pulse lengths. In contrast, for the low undercut depth $w_u = 0.9$ µm, even for very large outer radius geometries, laser emission is observed. As an example, Fig. 4c shows the emission spectra acquired from a diode with $w_u = 0.9$ µm, $r_i = 9$ µm and $R_o = 20$ µm under pumping with a 75 ns pulse length. The laser threshold is in this case $J_{th} = 24$ kA/cm^2. This behaviour is attributed to the heat generated during the pumping at high current injection and its dissipation path away from the GeSn WGM mode region, that includes heat transfer through the GeSn layer and through the Ge pedestal. The assumption is in agreement with recently reported experiments of the lattice thermal conductivity of GeSn layers, where the lattice thermal conductivity of a GeSn layer with 14 at.% of Sn was found to be as low as 5 W/m.K, one magnitude lower than pure Ge at 300 K [48].

To offer a quantitatively estimation of this assumption, the laser emission was investigated versus the pulse length (heating time) at constant pulse repetition rate. Fig. 5 shows the duty cycle-corrected emission of a diode ($w_u = 1.5$ µm, $R_o = 7$ µm) pumped above the threshold, with a constant 80 kA/cm^2 current density, 50 kHz repetition rate and pulse lengths of 100 ns, 150 ns, and 200 ns. A steady emission decrease with pulse length increment is observed, indicating quantum efficiency drop. This is attributed to the lattice heating and is in agreement with the LED intensity decrease with increasing temperature showed in Figs. 2a, c. Further reduction of the pulse length was also tested. Unfortunately, the current pulse shape suffers severe deformation below 75 ns due to parasitic capacitances of the cryostat circuits and pulse generator.

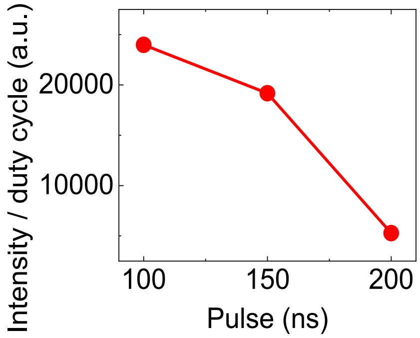

***Figure 5**: Duty cycle corrected intensity of 1.5 μm undercut diode at different pulse lengths and high current density of 80 kA/cm².*

Due to a reduced thermal effect, the laser emission of low underetch micro-rings, $w_u = 0.9$ μm, was extended to larger outer radius up to 40 μm, as shown in Fig. 6a. Increasing the diode outer radius from 6.5 μm to 40 μm, the threshold current density is significantly reduced from 60 kA/cm² to 10 kA/cm² (see Fig. 6b) . These laser diodes possess an increased GeSn to Ge pillar area ratio, which leads to a better heat distribution away from the GeSn active layer. As shown in Fig. 6c, for 0.9 μm undercut samples, this ratio positively correlates with the threshold current density.

The results presented in this work on small footprint DHS disk lasers, occupying an area of the order of 10^2 μm², can be compared with those reported by the group of Prof. Yu on edge-emitter FP lasers [40], [41], [43], whose length is in the mm range and the diode area is of $10^{4\text{-}5}$ μm². Both diodes successfully demonstrated laser emission under pulsed pumping condition (< 1 μs). The large edge emitters show lower one order lower laser threshold, J_{th} = ~1 kA/cm² but one magnitude higher total current (>1 A). These values, taken at 5K, are however, similar to the early stage values obtained for III-V lasers hetero-integrated on Si photonic chips, although the III-V devices operate in CW and at RT [49], [50], [51], [52], [53], [54], [55]. Both results demonstrate the potential and feasibility to monolithically integrate Si-based laser diodes on silicon chip with CMOS compatible group-IV material epitaxy technologies.

III. Conclusions

Electrical pumped micro-rings lasers using GeSn alloys of 14 at.% Sn content as gain medium and SiGeSn injection layers have been fabricated and characterized. The laser threshold strongly varies with the cavity undercut, geometrical dimensions and pumping pulse length. The heating effect was found to play an important role in the optical emission and leading to a lack of laser effect in large radius devices with with large undercut region. A reduced under-etching, that maintains a larger Ge pillar, allows lasing in large radius devices up to 40 μm radius and at a ~10-fold drop of threshold current density compared to 7 μm radius diodes. The work adds new information on cavity design role in laser emission and form the base for future design optimization for monolithically integrated laser diodes on Si.

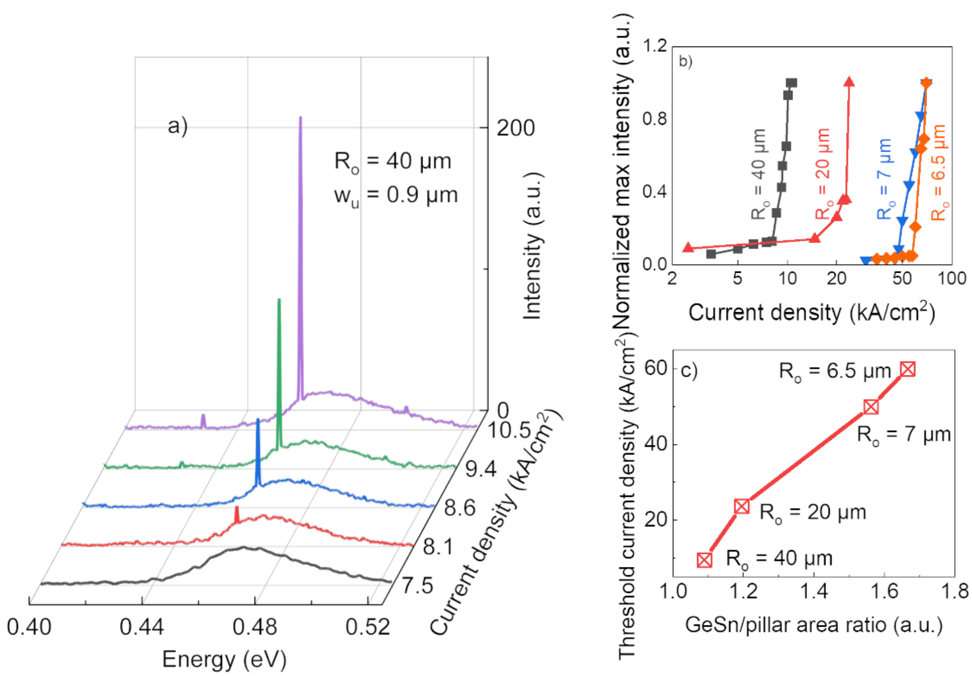

***Figure 6**: (a) 3D plot of EL spectra at 5K from a 40 μm radius diode for different current densities under 75 ns pulse pumping and 50 kHz repetition rate. (b) L-I characteristics of different outer radius diodes with an undercuting depth of 0.9 um and same operation mode as in (a). The intensity is normalized for a better comparison of the laser threshold. (c) Threshold current density as funcion of the GeSn cavitiy/Ge pillar area ratio indicating a strong correlation.*

METHODS

The GeSn/SiGeSn epitaxial heterostructure was grown in an AIXTRON reduced-pressure chemical-vapor-deposition reactor on a 200-mm Si (100) wafer buffered with a 1.7 µm-thick Ge layer in-situ boron-doped to 10^{18} cm^{-3}. N-type doping was achieved with in-situ phosphorus doping during the CVD epitaxy using PH_3 as gas precursor. Structures were then characterized by XRD confirming the as-grown compressive strain.

LED and laser cavities mesa were defined by HBr/Ar RIE process down to the germanium layer, followed by 600 nm SiO_2 passivation layer and metal contact process. To avoid possible Sn segregation, a low-temperature PECVD process (200 ºC) was deployed for the SiO_2 layer deposition. Undercut of germanium below GeSn cavities was achieved by a CF_4 RIE selective undercut process added after mesa definition [56], which anisotropic etched germanium with selectivity above 20:1.

Light emission spectrums were measured with a Bruker's Vertex 80v FTIR spectrometer using a step-scan mode to achieve higher signal to noise ratio. Resolution was set to 4 cm^{-1} or 1 cm^{-1} for the laser spectrum measurement, and 32 cm^{-1} for broad band LED spectrum measurements.

ACKNOWLEDGMENT

The authors acknowledge financial support from the European Commission for the LASTSTEP Project under grant agreement 101070208 and the German Research Foundation (DFG) under Projects "Thermoelektrische Eigenschaften von SiGeSn-Mikrobauelementen"

REFERENCES

[1] W. Q. Wei *et al.*, "Monolithic integration of embedded III-V lasers on SOI," *Light Sci Appl*, vol. 12, no. 1, 2023, doi: 10.1038/s41377-023-01128-z.

[2] W. Y. Ji *et al.*, "3 µ m InAs quantum well lasers at room temperature on InP," *Appl Phys Lett*, vol. 113, no. 23, 2018, doi: 10.1063/1.5050175.

[3] J. Witzens, "High-Speed Silicon Photonics Modulators," *Proceedings of the IEEE*, vol. 106, no. 12, 2018, doi: 10.1109/JPROC.2018.2877636.

[4] J. Wang, F. Sciarrino, A. Laing, and M. G. Thompson, "Integrated photonic quantum technologies," 2020. doi: 10.1038/s41566-019-0532-1.

[5] J. Yang, M. Tang, S. Chen, and H. Liu, "From past to future: on-chip laser sources for photonic integrated circuits," *Light Sci Appl*, vol. 12, no. 1, 2023, doi: 10.1038/s41377-022-01006-0.

[6] S. Shekhar *et al.*, "Roadmapping the next generation of silicon photonics," *Nat Commun*, vol. 15, no. 1, 2024, doi: 10.1038/s41467-024-44750-0.

[7] K. P. Homewood and M. A. Lourenço, "The rise of the GeSn laser," *Nat Photonics*, vol. 9, no. 2, 2015, doi: 10.1038/nphoton.2015.1.

[8] D. Stange *et al.*, "Optically Pumped GeSn Microdisk Lasers on Si," *ACS Photonics*, vol. 3, no. 7, 2016, doi: 10.1021/acsphotonics.6b00258.

[9] Y. Kim *et al.*, "Enhanced GeSn Microdisk Lasers Directly Released on Si," *Adv Opt Mater*, vol. 10, no. 2, 2022, doi: 10.1002/adom.202101213.

[10] S. Wirths *et al.*, "Lasing in direct-bandgap GeSn alloy grown on Si," *Nat Photonics*, vol. 9, no. 2, 2015, doi: 10.1038/nphoton.2014.321.

[11] A. Elbaz *et al.*, "Ultra-low-threshold continuous-wave and pulsed lasing in tensile-strained GeSn alloys," *Nat Photonics*, vol. 14, no. 6, 2020, doi: 10.1038/s41566-020-0601-5.

[12] Q. Chen *et al.*, "GeSn/Ge Multiquantum-Well Vertical-Cavity Surface-Emitting p-i-n Structures and Diode Emitters on a 200 mm Ge-on-Insulator Platform," *ACS Photonics*, vol. 10, no. 6, 2023, doi: 10.1021/acsphotonics.2c01934.

[13] Q. M. Thai *et al.*, "GeSn optical gain and lasing characteristics modelling," *Phys Rev B*, vol. 102, no. 15, 2020, doi: 10.1103/PhysRevB.102.155203.

[14] D. Rainko *et al.*, "Investigation of carrier confinement in direct bandgap GeSn/SiGeSn 2D and 0D heterostructures," *Sci Rep*, vol. 8, no. 1, 2018, doi: 10.1038/s41598-018-33820-1.

[15] F. T. Armand Pilon *et al.*, "Lasing in strained germanium microbridges," *Nat Commun*, vol. 10, no. 1, 2019, doi: 10.1038/s41467-019-10655-6.

[16] D. Rainko *et al.*, "Impact of tensile strain on low Sn content GeSn lasing," *Sci Rep*, vol. 9, no. 1, 2019, doi: 10.1038/s41598-018-36837-8.

[17] S. Gupta, B. Magyari-Köpe, Y. Nishi, and K. C. Saraswat, "Achieving direct band gap in germanium through integration of Sn alloying and external strain," *J Appl Phys*, vol. 113, no. 7, 2013, doi: 10.1063/1.4792649.

[18] H.-J. Joo *et al.*, "Actively tunable laser action in GeSn nanomechanical oscillators," *Nat Nanotechnol*, vol. 19, no. 8, pp. 1116–1121, 2024, doi: 10.1038/s41565-024-01662-w.

[19] J. Chrétien *et al.*, "GeSn Lasers Covering a Wide Wavelength Range Thanks to Uniaxial Tensile Strain," *ACS Photonics*, vol. 6, no. 10, 2019, doi: 10.1021/acsphotonics.9b00712.

[20] D. Burt *et al.*, "Tensile strained direct bandgap GeSn microbridges enabled in GeSn-on-insulator substrates with residual tensile strain," *Opt Lett*, vol. 48, no. 3, 2023, doi: 10.1364/ol.476517.

[21] D. Stange *et al.*, "GeSn/SiGeSn Heterostructure and Multi Quantum Well Lasers," *ACS Photonics*, vol. 5, no. 11, 2018, doi: 10.1021/acsphotonics.8b01116.

[22] N. von den Driesch *et al.*, "Advanced GeSn/SiGeSn Group IV Heterostructure Lasers," *Advanced Science*, vol. 5, no. 6, 2018, doi: 10.1002/advs.201700955.

[23] V. Reboud *et al.*, "Optically pumped GeSn micro-disks with 16% Sn lasing at 3.1 µ m up to 180 K," *Appl Phys Lett*, vol. 111, no. 9, 2017, doi: 10.1063/1.5000353.

[24] B. Wang *et al.*, "GeSnOI mid-infrared laser technology," *Light Sci Appl*, vol. 10, no. 1, 2021, doi: 10.1038/s41377-021-00675-7.

[25] Q. M. Thai *et al.*, "2D hexagonal photonic crystal GeSn laser with 16% Sn content," *Appl Phys Lett*, vol. 113, no. 5, 2018, doi: 10.1063/1.5036739.

[26] H. J. Joo *et al.*, "1D photonic crystal direct bandgap GeSn-on-insulator laser," *Appl Phys Lett*, vol. 119, no. 20, 2021, doi: 10.1063/5.0066935.

[27] H. J. Joo *et al.*, "All-Around HfO2 Stressor for Tensile Strain in GeSn-on-Insulator Nanobeam Lasers," *Adv Opt Mater*, vol. 11, no. 24, 2023, doi: 10.1002/adom.202301115.

[28] S. Al-Kabi *et al.*, "An optically pumped 2.5 μm GeSn laser on Si operating at 110 K," *Appl Phys Lett*, vol. 109, no. 17, p. 171105, Oct. 2016, doi: 10.1063/1.4966141.

[29] J. Margetis *et al.*, "Si-Based GeSn Lasers with Wavelength Coverage of 2-3 μm and Operating Temperatures up to 180 K," *ACS Photonics*, vol. 5, no. 3, 2018, doi: 10.1021/acsphotonics.7b00938.

[30] Y. Zhou *et al.*, "Optically Pumped GeSn Lasers Operating at 270 K with Broad Waveguide Structures on Si," *ACS Photonics*, vol. 6, no. 6, 2019, doi: 10.1021/acsphotonics.9b00030.

[31] G. Sun and S. Q. Yu, "The SiGeSn approach towards Si-based lasers," *Solid State Electron*, vol. 83, 2013, doi: 10.1016/j.sse.2013.01.037.

[32] N. Von Den Driesch *et al.*, "Direct Bandgap Group IV Epitaxy on Si for Laser Applications," *Chemistry of Materials*, vol. 27, no. 13, 2015, doi: 10.1021/acs.chemmater.5b01327.

[33] Q. M. Thai *et al.*, "GeSn heterostructure micro-disk laser operating at 230 K," *Opt Express*, vol. 26, no. 25, 2018, doi: 10.1364/oe.26.032500.

[34] A. Bjelajac *et al.*, "Up to 300 K lasing with GeSn-On-Insulator microdisk resonators," *Opt Express*, vol. 30, no. 3, 2022, doi: 10.1364/oe.449895.

[35] D. Buca *et al.*, "Room Temperature Lasing in GeSn Microdisks Enabled by Strain Engineering," *Adv Opt Mater*, vol. 10, no. 22, 2022, doi: 10.1002/adom.202201024.

[36] Y. Junk *et al.*, "Enhancing Device Performance with High Electron Mobility GeSn Materials," *Adv Electron Mater*, vol. n/a, no. n/a, p. 2400561, Aug. 2024, doi: https://doi.org/10.1002/aelm.202400561.

[37] M. Liu *et al.*, "Vertical GeSn nanowire MOSFETs for CMOS beyond silicon," *Communications Engineering*, vol. 2, no. 1, 2023, doi: 10.1038/s44172-023-00059-2.

[38] M. Liu *et al.*, "Epitaxial GeSn/Ge Vertical Nanowires for p-Type Field-Effect Transistors with Enhanced Performance," *ACS Appl Nano Mater*, vol. 4, no. 1, 2021, doi: 10.1021/acsanm.0c02368.

[39] Y. Chuang, C. Y. Liu, H. S. Kao, K. Y. Tien, G. L. Luo, and J. Y. Li, "Schottky Barrier Height Modulation of Metal/n-GeSn Contacts Featuring Low Contact Resistivity by in Situ Chemical Vapor Deposition Doping and NiGeSn Alloy Formation," *ACS Appl Electron Mater*, vol. 3, no. 3, 2021, doi: 10.1021/acsaelm.0c01108.

[40] Y. Zhou *et al.*, "Electrically injected GeSn lasers on Si operating up to 100 K," *Optica*, vol. 7, no. 8, pp. 924–928, Aug. 2020, doi: 10.1364/OPTICA.395687.

[41] Y. Zhou *et al.*, "Electrically injected GeSn lasers with peak wavelength up to 2.7 μm," *Photonics Res*, vol. 10, no. 1, 2022, doi: 10.1364/prj.443144.

[42] B. Marzban *et al.*, "Strain Engineered Electrically Pumped SiGeSn Microring Lasers on Si," *ACS Photonics*, vol. 10, no. 1, 2023, doi: 10.1021/acsphotonics.2c01508.

[43] G. Abernathy *et al.*, "Study of all-group-IV SiGeSn mid-IR lasers with dual wavelength emission," *Sci Rep*, vol. 13, no. 1, 2023, doi: 10.1038/s41598-023-45916-4.

[44] T. B. Bahder, "Eight-band kp model of strained zinc-blende crystals," *Phys Rev B*, vol. 41, no. 17, 1990, doi: 10.1103/PhysRevB.41.11992.

[45] M. Bertrand *et al.*, "Experimental Calibration of Sn-Related Varshni Parameters for High Sn Content GeSn Layers," *Ann Phys*, vol. 531, no. 6, 2019, doi: 10.1002/andp.201800396.

[46] C. Corley-Wiciak *et al.*, "Full Picture of Lattice Deformation in a Ge1 − xSnx Micro-Disk by 5D X-ray Diffraction Microscopy," *Small Methods*, vol. n/a, no. n/a, p. 2400598, Jul. 2024, doi: https://doi.org/10.1002/smtd.202400598.

[47] H. Tran *et al.*, "Systematic study of Ge1-xSnx absorption coefficient and refractive index for the device applications of Si-based optoelectronics," *J Appl Phys*, vol. 119, no. 10, 2016, doi: 10.1063/1.4943652.

[48] O. Concepción *et al.*, "Room Temperature Lattice Thermal Conductivity of GeSn Alloys," *ACS Appl Energy Mater*, vol. 7, no. 10, pp. 4394–4401, May 2024, doi: 10.1021/acsaem.4c00275.

[49] J. Zhang, Y. Li, S. Dhoore, G. Morthier, and G. Roelkens, "Unidirectional, widely-tunable and narrow-linewidth heterogeneously integrated III-V-on-silicon laser," *Opt Express*, vol. 25, no. 6, 2017, doi: 10.1364/oe.25.007092.

[50] B. Shi, S. Pinna, H. Zhao, S. Zhu, and J. Klamkin, "Lasing Characteristics and Reliability of 1550 nm Laser Diodes Monolithically Grown on Silicon," *Physica Status Solidi (A) Applications and Materials Science*, vol. 218, no. 3, 2021, doi: 10.1002/pssa.202000374.

[51] N. Li *et al.*, "Integrated Lasers on Silicon at Communication Wavelength: A Progress Review," 2022. doi: 10.1002/adom.202201008.

[52] M. Feng, J. Liu, Q. Sun, and H. Yang, "III-nitride semiconductor lasers grown on Si," 2021. doi: 10.1016/j.pquantelec.2021.100323.

[53] M. Tang *et al.*, "Integration of III-V lasers on Si for Si photonics," 2019. doi: 10.1016/j.pquantelec.2019.05.002.

[54] E. Tournié *et al.*, "Mid-infrared III–V semiconductor lasers epitaxially grown on Si

substrates," 2022. doi: 10.1038/s41377-022-00850-4.
[55] Y. Wan *et al.*, "High Speed Evanescent Quantum-Dot Lasers on Si," *Laser Photon Rev*, vol. 15, no. 8, 2021, doi: 10.1002/lpor.202100057.
[56] S. Gupta *et al.*, "Highly Selective Dry Etching of Germanium over Germanium–Tin (Ge1–xSnx): A Novel Route for Ge1–xSnx Nanostructure Fabrication," *Nano Lett*, vol. 13, no. 8, pp. 3783–3790, Jul. 2013, doi: 10.1021/nl4017286.

Teren Liu is a Ph.D. candidate in "Si-based Epitaxy and Photonics" group of Peter-Grünberg-Institute (PGI-9) , Forschungzentrum Jülich, Germany. He received his Bachelor of Engineering degree in opto-electronic science and technology from Harbin Institute of Technology, China and M.A.Sc in Materials Engineering from the University of British Columbia, Canada. His research focused on the fabrication and characterization of GeSn/SiGeSn based opto-electronic devices on silicon, including LED/laser diodes, and photodetectors.

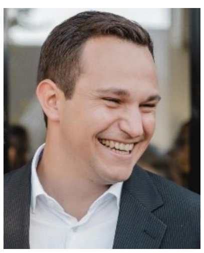

Lukas Seidel was born in Ulm, Germany in 1995. He received his B. Sc. degree in Electrical Engineering and Information Technology (2017) and M. Sc. degrees in Photonic Engineering (2020) from the University of Stuttgart, Germany. He is currently pursuing his Ph. D. degree in Electrical Engineering at the Institute of Semiconductor Engineering at the University of Stuttgart. He is mainly engaged in the research of group IV photonics and focused on integrable Silicon-Germanium-Tin lasers.

Omar Concepción received a master degree in Physics from the University of Havana, Cuba in 2015 and the Ph.D. degree in Nanoscience and Nanotechnology from Cinvestav-IPN, Mexico in 2018. From 2018 to 2021, he joined the University of Twente, The Netherlands working in the epitaxy of topological insulator materials. Currently, he is Scientific Researcher in Peter Gruenberg Institute 9 – Semiconductor Materials at Research Center Jülich (Forschungszentrum Jülich), in the group of Silicon-based epitaxy and photonics. His research focuses on the epitaxial growth of all-group-IV materials by industry-compatible CVD for photonics, nanoelectronic, energy harvesting, and spintronics applications

Vincent Reboud received his PhD in Physics in 2004 from the University of Paris-Sud, Orsay, France. He joined after the Tyndall National Institute in Ireland and then the Catalan Institute of Nanotechnology in Spain to study three dimensional and reconfigurable optical surfaces. He worked after on optoelectronic components patterned by wafer-scale nanoimprint lithography at CEA-LETI, France. In 2014, he joined the Silicon Photonics and then the Optical Sensing Lab of CEA-LETI as a senior scientist to work on IR & MIR photonics platform for a broad range of applications, especially lately on group-IV light sources and detectors for optical gas sensors.

Alexei Chelnokov/Tchelnokov received the Ph.D. and HDR (Habilitation) degrees, both from the University of Paris-South. He is currently the Chief Scientist of the Optics and Photonics Department, CEA-LETI (Grenoble, France), and one of its Directors of Research. Formerly, he was Heading several optoelectronics-oriented labs of the CEA-LETI. He was educated with the A.F. Ioffe Physico-Technical Institute (St.-Petersburg, Russia) and was with Ioffe Institute, CNRS Institute of Fundamental Electronics (Orsay, France), and Corning Inc. (France), with short stays with Polaroid Corp (MA, USA) and Thomson LCR (France). His research interests concern optoelectronic devices for tele- and data-communication, silicon photonics, solid-state light-emitting devices, and nano-optics.

Giovanni Capellini graduated in Physics from the University of Rome La Sapienza in 1994 and obtained his Ph.D. in Physics from the University of Rome Tor Vergatain 1998. In 2002 he joined Luxtera Inc. (Carlsbad CA, USA)- and the California Institute of Technology in Pasadena, California as Visiting Associate Professor. Since 2018 he is Full Professor of Condensed Matter Physics at the Dept. of Sciences of Roma Tre University and Senior Scientist at the Leibniz Institute Innovations for High Performance Microelectronics Frankfurt Oder, Germany. His main field of interest is the development of innovative nanostructured materials with potential applications in optoelectronics, nanophotonics. and biosensing devices.

Michael Oehme received the Dipl.-Phys. degree from the Institute of Physics, University of Jena, Jena, Germany, in 1997. In 2003, he received the Ph.D. degree in electrical engineering with a dissertation on the determination of doping concentrations from the University of Stuttgart.

He is senior researcher at the institute of semiconductor engineering at the University of

Stuttgart. His research interests include epitaxial growth of group IV materials on Si, group IV photonics, nanoelectronics, and quantum electronics.

Detlev Grützmacher received the Diploma in physics from the Institute of Semiconductor Electronics, Aachen, Germany, and the Ph.D. degree (with special honors) from the University of Aachen, Achen, in 1991. In May 2001, he defended the Habilitation at the University of Konstanz, Germany. From 1991 to 1993, he was a Postdoctoral Fellow at the IBM Thomas Watson Research Center, Yorktown Heights, NY. In 1993, he joined the Laboratory of Micro- and Nanotechnology at the Paul Scherrer Institute, Villigen, Switzerland, where he currently heads the Si nanosystems activity focusing on Si-Ge nanostructures for optoelectronic and electronic applications. Dr. Grützmacher received the Borchers Medal of the University of Aachen, in 1991. He also received the IBM Research Division Award, in 1992, and a Patent Invention Award, in 1993, for his research on high-speed hetero-bipolar transistors as well as resonant tunnelling devices. He is now the institute director of Peter-Grünberg-Institute (PGI-9) , Forschungzentrum Jülich.

Dan Buca received the Master degree in Physics from the Faculty of Physics, University of Bucharest, Romania in 1999. In 2002, he received the Ph.D. degree in Physics from the University of Cologne, Germany with a dissertation on the SiGe photodetectors. Dr. Buca is senior scientist and leader of the “Si-based Epitaxy and Photonics” group at the Peter Gruenberg Institute 9 – Semiconductor Materials at Research Center Jülich (Forschungszentrum Jülich). His research interests include epitaxial growth of group IV materials and their applications in photonics, nanoelectronics, quantum transport and energy harvesting.